Chemical Engineering Journal 336 (2018) 160–169

Contents lists available at ScienceDirect

Chemical Engineering Journal

journal homepage: www.elsevier.com/locate/cej

Sustainable efficient adsorbent: Alkali-acid modified magnetic biochar derived from sewage sludge for aqueous organic contaminant removal

Lin Tang[a,c,*], Jiangfang Yu[a,c], Ya Pang[b,*], Guangming Zeng[a,c], Yaocheng Deng[a,c], Jiajia Wang[a,c], Xiaoya Ren[a,c], Shujing Ye[a,c], Bo Peng[a,c], Haopeng Feng[a,c]

[a] College of Environmental Science and Engineering, Hunan University, Changsha 410082, China
[b] Department of Biology and Environmental Engineering, Changsha College, Changsha 410003, Hunan, China
[c] Key Laboratory of Environmental Biology and Pollution Control (Hunan University), Ministry of Education, Changsha 410082, Hunan, China

GRAPHICAL ABSTRACT

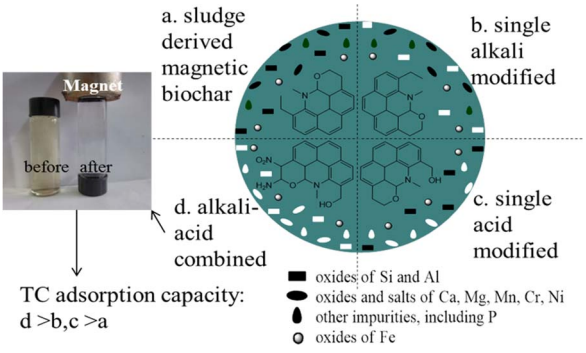

ARTICLE INFO

Keywords:
Municipal sewage sludge
Effective modified biochar
Tetracycline removal
Magnetic separation
Mechanism
Large-scale application potential

ABSTRACT

Municipal sewage sludge (MS)-derived biochar shows low-cost superiority as a potential adsorbent in organic contaminants removal, but limited by its poor adsorption capacity and heavy metal leaking risk. Herein, a novel and effective alkali-acid combined method was proposed for its modification and applied to tetracycline adsorption. The associative facilitation between the alkali and acid modifications was explored, and the influences of pyrolysis temperatures on MS-biochar's properties were investigated. The successfully preserved γ-Fe_2O_3 vested SNMS-800 with magnetism. It turned out that SNMS-800 exhibited optimum performance for tetracycline removal with adsorption capacity up to 286.913 mg/g, where all goodness-of-fit indexes of isothermal models were measured by MPSD model. The strong adsorption mechanisms were dominated by two considerable interactions, including strong π-π stacking interaction and pore-filling effect due to the significantly enhanced porosity which was proved by density functional theory model calculations. It manifested that appropriate multiple relation (1.7–6 times) between adsorbent's pore size and adsorbate size closely related to the adsorption strength. The remarkably improved and stable adsorption capacity, extremely low-cost, easy magnetic preparation, and good reusability in natural water samples entrusted SNMS-800 with good potential for actual aqueous contaminant removal on a large scale. Meanwhile, it provides a clue for materials modification starting with its specific components, and supplies a cost-effective way for municipal sewage sludge's resource disposal.

* Corresponding authors at: College of Environmental Science and Engineering, Hunan University, Changsha, China (L. Tang). Department of Biology and Environmental Engineering, Changsha College, Changsha, Hunan, China (Y. Pang).
E-mail addresses: tanglin@hnu.edu.cn (L. Tang), pangya0989@ccsu.edu.cn (Y. Pang).

https://doi.org/10.1016/j.cej.2017.11.048
Received 2 September 2017; Received in revised form 7 November 2017; Accepted 8 November 2017
Available online 09 November 2017
1385-8947/

1. Introduction

Nowadays, various technologies have been reported to eliminate aqueous organic contaminants, such as adsorption, photolysis, chemical oxidation and biodegradation [1]. Among them, adsorption is considered as a cost-effective and wide available method. However, as the common adsorbent widely used for water remediation, activated carbon [2] and carbon nanotubes are relatively expensive in practice, and difficult for separation recycling. The seeking of economical, high-efficiency, sustainable, green and easily separable adsorbent is still necessary for adsorption application. Biochar, a carbon-rich solid which is prepared by biomass thermal decomposition under an oxygen-deficient environment, usually possesses abundant pore structures and relatively rich functional groups [3], entrusting it with adsorption properties. Due to the wide range of biomass materials, including agriculture and forestry residues, animal litters and other solid wastes [4,5], biochar shows low-cost superiority over many other adsorbents. Moreover, because of the win-win effects of water remediation and carbon sequestration, considerable attention has been paid to investigating aqueous contaminants removal by biochar. However, the adsorptive property of biochar relies much on its raw material and calcination temperature [6].

As a major by-product of municipal sewage treatment plant, municipal sewage sludge (MS) is regarded as a pollutant and usually to be burnt or buried in the landfill [7], which could easily cause secondary pollution and resources wasting. And its abundant organic matter vests MS with potential for biochar preparation. Nevertheless, on account of the limited porosity and functional groups, the pristine MS-biochar shows poor adsorption capacity for both organic pollutants and heavy metals. Therefore, appropriate modification is necessary for MS-biochar. It has been reported that MS-biochar modified with $CaCO_3$ after pyrolysis could enhance its cadmium adsorption capacity to 36.5 mg/g [8]. Magnetic MS-biochar with the surface area of 40.96 m^2/g prepared with impregnation method showed relative good lead adsorption ability [9]. And the alkali-pretreated MS-biochar showed a higher cadmium adsorption capacity (0.713 mmol/g) than that without pre-treatment [10]. However, the adsorption properties of these single-modified MS-biochars are still unsatisfactory, and few reports have taken the secondary pollution risk into consideration, namely the possible impurities leaking from MS-biochar into water, such as heavy metals stemmed from sewage sludge itself [11], especially under acidic condition.

Generally, most of the inorganic salts in MS-based carbon materials, such as the oxides and salts of Ca, Mg, Mn, Fe, Pb, Cd, Ni and Cr, could be removed by concentrated acid to form soluble ions, including HF which is hyper-toxic, highly volatile and not applicable to mass production [12]. Additionally, MS-based carbon materials usually contain a large number of silicon, which could be regarded as natural template and removed with thick hot alkali solution [13]. Theoretically, the expunged substances could bring abundant porosity, and the amount and types of surface functional groups would also increase [14]. As for adsorbent, its enhanced porosity and richer functional groups fatefully endow its stronger adsorption ability [15]. Therefore, based on the special components of municipal sewage sludge, a novel method, alkali-acid combined modification for MS-biochar, is considered to be a promising approach to enhance the adsorption property efficiently.

What's more, as for carbon adsorbents scattered in the water, their effective separation and recycling could be a challenge. Generally, MS obtained from municipal wastewater treatment was added with flocculants, and PAM (polyacrylamide) combined with PFC (polyferric chloride) or PFS (polyferric sulfate) are the most commonly used [16], where the additive PFC or PFS could be regarded as iron resources. And in this study, the dehydrated MS obtained from municipal sewage plant was already flocculated with PAM and PFS. The additive PFS could impart MS-biochar with magnetism, which could be the effective countermeasures for its recycling challenge. Different from magnetic MS-biochars prepared with impregnation method after pyrolysis where magnetic particles distributed on the biochar surface are easy to fall off or be corroded, the magnetic particles in this study would be well wrapped by carbon due to the full mixing of PFS and sludge during flocculation process before pyrolysis, and could endow MS-biochar with good magnetic retention. However, iron oxides could be removed easily by many acids. In order to preserve MS-biochar's magnetism, concentrated nitric acid based on its passivation with iron, and acetic acid on account of its faintly acid were applied for acid modification with the operating temperature under 15 °C at limited time, respectively.

Hence, in this work, in order to prepare an environmentally friendly, economic, highly efficient and magnetic MS-biochar, we have been dedicated to develop a novel alkali-acid combined method for magnetic MS-biochar modification. And the interaction between the alkali and acid modifications and possible adsorption mechanisms were explored. The influence of pyrolysis temperatures and resulted material structures were investigated in detail. And the obtained biochar was applied for tetracycline (TC) removal which was a versatile broad spectrum bacteriostatic antibiotic and was frequently detected from aquatic environment, and its adsorption mechanism was first investigated. Strong adsorption ability for TC in natural water by the proposed material was found with good stability and reusability. This study has provided a novel and feasible approach to prepare a cost-effective magnetic MS-biochar for antibiotics contaminated water treatment, and its excellent properties entrusted magnetic MS-biochar with great potential for actual water purification on a large scale, which could be an effective way for sewage sludge disposal.

2. Materials and methods

2.1. Materials

Municipal sewage sludge (MS) was obtained from Xingsha Wastewater Treatment Plant, located in Changsha, China. Tetracycline hydrochloride (TC: purity > 98.5%), NaOH, HNO_3 (> 65%) and CH_3COOH (> 98%) were purchased from Shanghai Chemical Corp and used without further purification. The rice husk straw biochar (RS-biochar) was bought from Shouguangheneng biotechnology Co., Ltd, located in Shandong, China. Deionized water (18.25 MΩ/cm) generated by an Ulupure (UPRII-10 T) laboratory water system was used to prepare reaction solutions.

2.2. Adsorbents preparation

After drying, municipal sewage sludge (MS) was screened by 100 mesh sieve (0.15 mm) and calcined in a tubular reactor (SK-G04123K, China) for 2 h under nitrogen protection with heating rate of 5 °C/min. The MS-biochars obtained from different pyrolysis temperatures, including 400, 600 and 800 °C, were labelled as MS-400, MS-600 and MS-800, respectively. And MS-biochars was firstly modified with sodalye (2 M) at 90 °C for 2 h with water bath stirring, and then treated with concentrated nitric acid (14 M) (SNMS-biochar) or glacial acetic acid (17.2 M) (SAMS-biochar) during 10–15 °C for 2 h with magnetic stirring, where all the acid reagents were used as purchased without dilution. For comparison, MS-biochar only modified with sodalye (or nitric acid or acetic acid) was prepared and recorded as SMS-biochar (or NMS-biochar or AMS-biochar).

2.3. Analytical methods

The morphology was observed by the scanning electron microscope (SEM, Zeiss Merlin) and transmission electron microscopy (TEM, JEM-2010). The porosity was determined by nitrogen adsorption-desorption conducted on a Micromeritics 2020 analyzer at 77 K. X-ray diffraction (XRD) and X-ray photoelectron spectroscopy (XPS, Thermo Fisher Scientific) served for the element composition determination. The existing functional groups were detected by the Fourier transform infrared

spectrometer (FTIR, Nicolet Magna-IR 750). The zeta potentials and the hydraulics particle size were measured on a Zetasizer Nano (ZEN3600, Malvern). UV–VIS diffuse-reflectance spectra (UV–vis DRS) were recorded in the range of 200–800 nm with a Varian Cary 300 spectrometer. The total organic carbon (TOC) analysis was conducted by a Shimadzu TOC-VCPH analyzer. Three-dimensional excitation-emission matrix fluorescence spectra (3D EEMs) were taken with the excitation wavelengths range from 200 nm to 450 nm, and the emission wavelengths ranged from 300 nm to 550 nm. The material's magnetic property was studied by a vibrating sample magnetometer (VSM) at room temperature. The characterization of used water samples were analyzed by Inductively Coupled Plasma Optical Emission Spectrometer (ICP-OES).

2.4. Batch adsorption experiments

1000 mg/L TC was used as stock solution and stored in a brown volumetric flask at 4 °C, and were diluted to specific concentrations (50–800 mg/L) for experiment. 20 mg adsorbent was adding to 20 mL TC solution shaking at 160 rpm. The influence factors, including contact time, pH, initial TC concentration, adsorption temperature and ionic strength, were taken into account. All samples were filtered with a 0.45 μm filter which was proved to have no intercepting effects for the TC molecule, and then analyzed by a UV–VIS absorbance at 357 nm, necessarily assisted with TOC analysis.

Detailed information about all calculation equations and models, including isotherm models, kinetics models and thermodynamic models in this study were shown in Table S1 [17–19]. Due to the limitation of coefficient values in estimation of the fitting degree of models, Marquardt's percent standard deviation (MPSD) model was applied for goodness-of-fit index judgement [20].

2.5. Application on natural water and regenerability

To evaluate the performance of magnetic MS-biochar for TC adsorption in different water samples, deionized water, tap water and lake water obtained from Peach Lake located in Changsha were applied for investigation, which were directly applied for TC solution preparation without filtration. During the reaction process, the samples used for TC concentration analysis were filtered by 0.45 μm filter. And their characterization before and after filtration were shown in Table S2, demonstrating that the filtration showed little influence on element content of water samples. The decreased TOC value of lake water after filtration might be ascribed to the removal of intercepted natural floccus.

Apart from SNMS-800, RS-biochar and MS-800 were tested for comparison. Additionally, the TC-loaded SNMS-800 was added to 0.2 M NaOH solution, stirred at 298 K for 4 h, then replaced with fresh NaOH solution and stirred for another 4 h for completely desorption. The regenerative SNMS-biochar was washed, dried and applied for next adsorption experiment.

3. Resutls and discussion

3.1. Effects of different modification methods

SEM (shown in Fig. 1a–d) manifested the morphology changes of the MS-biochars after different modifications. As for MS-800, it owned irregular surface where many impurity particles were distributed on, and no distinct pores could be observed. However, SMS-800 showed an obvious changed surface with many sheet structures which might be ascribed to the interaction between sodium hydrate and impurity particles. More importantly, after further modification with nitric acid, abundant noticeable pore structures could be observed easily on SNMS-800 which might stem from the sites of impurities indicating their successful removal. Nevertheless, as for SAMS-800, the enhanced pore

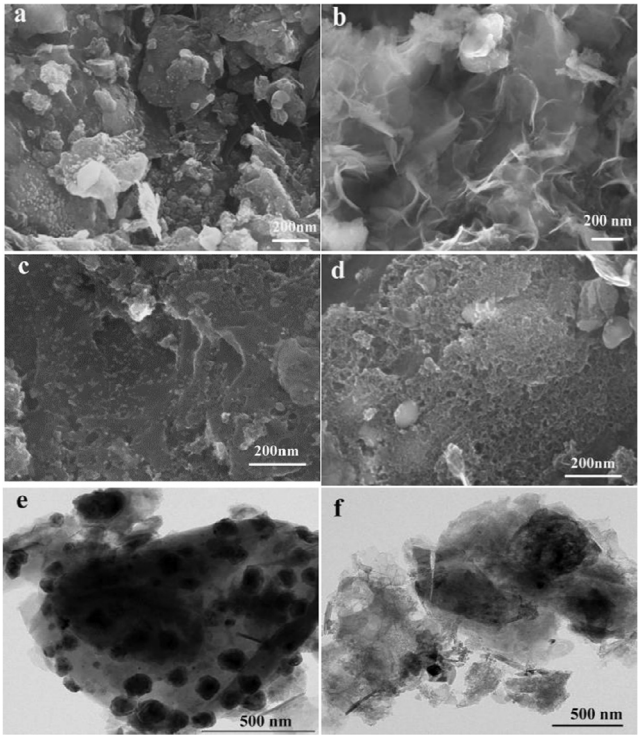

Fig. 1. SEM patterns of MS-800 (**a**), SMS-800 (**b**), SAMS-800 (**c**) and SNMS-800 (**d**), TEM patterns of MS-800 (**e**) and SNMS-800 (**f**).

structures was not so obvious as SNMS-800, demonstrating that different acids used in modification would affect sludge biochar properties. Additionally, compared to MS-800, the conspicuously decreased particles in SNMS-800 revealed by TEM (shown in Fig. 1e–f) demonstrated that alkali-acid combined method was effective for MS-biochar's purification to become environmental friendly.

The obviously changed surface morphology directly relate to biochars' porosity, which was verified by nitrogen adsorption-desorption analysis. According to Table 1, MS-800 showed a limited porosity with low BET area (67.387 m^2/g) and little pore volume (0.08835 cc/g), which might be the primary cause of its weak TC adsorption. While the BET of SNMS-800 (202.519 m^2/g) was three times of that of MS-800 with the total pore volume increasing to 0.2563 cc/g. And SNMS-biochar showed a superior porosity to SAMS-biochar. In order to investigate the integrated effect of alkali-acid combined modification on sludge biochars, single acid and alkali modifications were carried out and analyzed for comparison. As for single modification systems, alkali mostly enhanced the porosity (co-increased BET and pore volume), and nitric acid came to the second. But AMS-800 exhibited a slightly decreased BET which might be ascribed to the weak acidity of acetic acid along with the weak impurities removal ability. Compared with the single modification systems, the alkali-acid combined modified biochars possessed much higher BET and pore volume growth rates, demonstrating the associative facilitation for porosity between alkali modification and acid modification, which was more remarkable between alkali and acetic acid. And the associative facilitation might be attributed to that the anterior alkali modification could provide more exposed sites for the following acid treatment. Certainly, the increased BET and pore volume could accelerate adsorption ability.

However, appropriate pore size distribution of adsorbents also matters. According to the adsorption theory, it is believed that adsorbent shows its best adsorption property when pore diameter is 1.7–3 times larger than that of the adsorbate molecule. If regeneration is needed, it should be 3–6 times larger or even more [21]. Therefore, as shown in Fig. 2, density functional theory (DFT) calculations were used for pore size distribution analysis, which was based on balance density

Table 1
Porosity characteristic of municipal surplus sludge magnetic biochar.

Classifications	Materials	BJH Pore Diameter (nm)	BET Surface Area		Total Pore Volume (PV)		Q_e for TC (C_0 = 100 mg/L)
			BET (m^2/g)	Growth rate	PV (cc/g)	Growth rate	
MS-biochars without modification (MS)	MS-400	3.7324	39.077	–	0.0676	–	32.592
	MS-600	3.7222	43.578	–	0.0742	–	41.176
	MS-800	3.7382	67.387	–	0.08835	–	48.928
MS-biochars modified with sodalye and nitric acid (SNMS)	SNMS-400	3.3074	37.594	0.962	0.09325	1.3794	18.72
	SNMS-600	3.8904	153.719	3.5274	0.1861	2.5081	82.24
	SNMS-800	3.8618	202.519	3.0053	0.2563	2.901	91.436
MS-biochars modified with sodalye and glacial acetic acid (SAMS)	SAMS-400	3.634	24.484	0.6266	0.05091	0.7531	21.232
	SAMS-600	3.8946	151.644	3.4798	0.1891	2.5485	79.112
	SAMS-800	3.865	180.917	2.6847	0.2265	2.5637	90.684
MS-800 single modified with sodalye (SMS) or nitric acid (NMS) or glacial acetic acid (AMS)	SMS-800	3.9014	141.776	2.1039	0.207	2.343	78.6
	NMS-800	3.8792	102.385	1.5194	0.1463	1.6559	60.416
	AMS-800	3.8694	58.923	0.8744	0.1101	1.2462	23.648

for all positions of pores calculated by free energy function, exhibiting its accuracy superiority for materials combined with micropores ($r < 1$ nm) and mesopores (1 nm $< r <$ 25 nm), such as MS-biochar, than conventional Barrett-Joyner-Halenda method. Compared to MS-800, the apparently enriched channel numbers of modified biochars could be observed, where micropores might originate from impurity removal and mesopores mainly stemmed from the expansion of micropores. And as a macromolecular adsorbate, TC molecule with a three-dimensional structure of 1.41 nm long, 0.46 nm wide and 0.82 nm high [22], could be effectively adsorbed by pores with the radius ranging from 1.2 to 4.23 nm, which was just in the main channel distribution of modified MS-biochars to entrust with the high TC adsorption capacity. Perceptibly, the enhanced porosity with appropriate pore size distribution of sludge biochars showed a positive correlation with its TC adsorption capacity, demonstrating porosity was a crucial factor for TC adsorption by sludge biochar.

To further investigate the influence of the alkali-acid combined modification on sludge biochars adsorption properties, another critical factor, surface function groups, were illustrated by FTIR spectra. As shown in Fig. 3a, apart from common characteristic peaks centered around 692 cm^{-1} ($-CH_2-$), 781 cm^{-1} (C—H on carbon ring), 472 cm^{-1} (Fe_2O_3 and Si—O), 557 cm^{-1} (Fe-OH) and 1041 cm^{-1} (C—O, C—N and Si—O), the co-occurrences of peaks at 1539 cm^{-1} and 1604 cm^{-1} belonging to the vibration of C = C on the aromatic ring are more momentous, which can certify the existence of aromatic nucleus. As for the single modification system (Figure S1b), except NMS-800 showing emerging oxygen-containing groups (O—H) ranging around 3000 cm^{-1} to 3500 cm^{-1}, SMS-800 and AMS-800 showed little change. However, the alkali-acid combined modification system (Fig. 3a) showed the difference. Compared to MS-800, the new broad peak ranging from 3000 cm^{-1} to 3600 cm^{-1} (O—H) emerged on both SNMS-800 and SAMS-800. And another fresh peak for SNMS-800 at 3736 cm^{-1} derived from the oscillation of N—H was observed. The results indicated that alkali-acid combined system was more beneficial to the enrichment of functional groups. Additionally, as for SNMS-800-TC loaded with TC, the enhanced and widened peak around 3500 cm^{-1} to 3900 cm^{-1} was probably attributed to the incremental functional groups from TC molecule, demonstrating the successful adsorption of TC.

The adsorbents' components are highly related to the adsorption application, while magnetic separation capacity is vital for adsorbents' separation and recovery. Therefore, after the alkali-acid combined modification, the reservation of carbon and magnetic components really matters. According to the XRD patterns in the range of 3–80° shown in Fig. 3b, it is illuminated that the main components of the sludge biochars were carbon, quartz, iron oxide and aluminum oxide. Compared with MS-800, the intensity of the carbon peak on SNMS-800 was greatly enhanced. However, the peaks of quartz on SNMS-800 were still subsistent, which was mainly ascribed to the incomplete removal of quartz. The detection of γ-Fe_2O_3 emerged with stronger intensity indicating the increased content of iron oxide probably due to other impurities removal. And the successfully reserved γ-Fe_2O_3 endowed sludge biochar with good magnetism (shown in Video S1). Different from iron source which was loaded at the materials' surface by immersion method after calcination in other magnetic materials' preparation, the Fe element was distributed inside the sludge biochar (proved by SEM study) which was hybrid in situ before pyrolysis and hard to fall off or be corroded. This is very favorable to keep the magnetism longer and more stable.

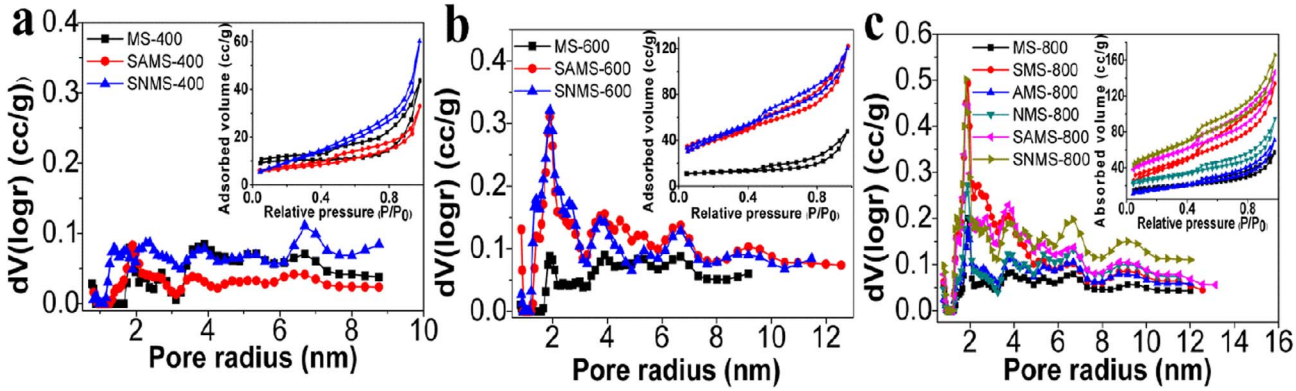

Fig. 2. Nitrogen adsorption-desorption isothermals and pore size distribution of magnetic MS-biochars calcined at 400 °C (**a**), 600 °C (**b**) and 800 °C (**c**) analyzed by DFT calculation.

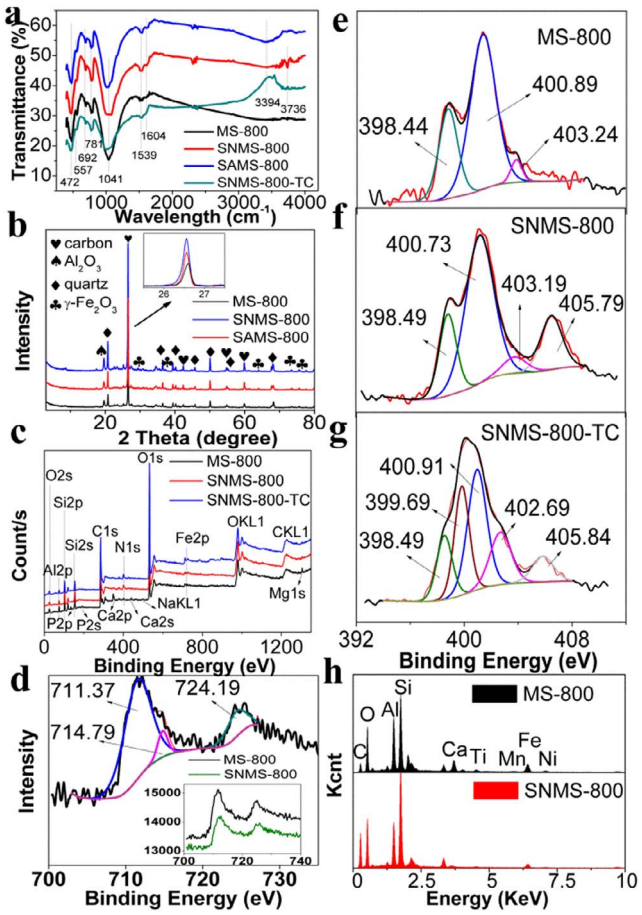

Fig. 3. FTIR spectrogram of MS-biochars (**a**), XRD patterns of MS-800, SAMS-800 and SNMS-800 (**b**), XPS full scan spectra of MS-800, SNMS-800 and SNMS-800-TC (**c**), Fe2p XPS spectrum of MS-800 and SNMS-800 (**d**), N1s XPS spectrum of MS-800 (**e**), SAMS-800 (**f**) and SNMS-800-TC (**g**), EDX spectra of MS-800 and SNMS-800 (**h**).

Video S1. The magnetic separation capacity of SNMS-800. The magnetic separation capacity of SNMS-800 can be found, in the online version, at http://dx.doi.org/10.1016/j.cej.2017.11.048.

XPS was applied for further component analysis, and the full scan spectrum was presented in Fig. 3c, revealed the main composition elements of the materials were C, O, Si, N, Fe and Al, which were consistent with the XRD results. Besides, in comparison to MS-800, the missing peaks of Ca2p (347.38 eV), Ca2s (441.0 eV), P2s (191.7 eV), P2p (133.4 eV), Mg1s (1303.96 eV), K2s (380 eV), NaKL1 (1501.79 eV) on SNMS-800 were attributed to the alkali-acid modification, manifesting their successful removal. Additionally, it turned out that the carbon of MS-800 mainly existed in graphite form with peak around 284 eV. The detailed XPS spectra of the specific elements, including Fe2p and N1s, were exhibited in Fig. 3d–g. As for Fe2p, little variation between MS-800 and SNMS-800 could be found, and the results demonstrated the existence of three types of iron-compounds, including dominating γ-Fe_2O_3 (2p3/2, 711.37 eV), ferric salt (2p3/2, 714.79 eV), and FeOOH (2p1/2, 724.19 eV). And their possible formation mechanisms were shown as below:

$$Fe^{3+} + 3H_2O \rightarrow Fe(OH)_3 + 3H^+$$

$$Fe(OH)_3 \rightarrow FeO(OH) + H_2O$$

$$2Fe(OH)_3 \rightarrow Fe_2O_3 + 3H_2O$$

As for N1s analysis, the common peaks around 398.44 eV and 400.8 eV represented pyridine nitrogen and pyrrole nitrogen, respectively. Compared with MS-800, the stronger peak around 402.69–403.24 eV might be ascribed to pyridine nitrogen which was mainly formed by oxidation of marginal pyridine or pyrrole nitrogen. And the new peak at 405.79 eV emerged on SNMS-800, which might be due to the addition of -NO_2 group. Another newly-presented peak at 399.69 eV of SNMS-800-TC might be attributed to the N—H on benzene ring from the adsorbed TC. Analogously, the fairly strong peak at 402.69 eV pointed to the substance of $C_xH_yCl_vNO_z$, which proved the successful adsorption of TC molecular. Additionally, as verified by EDX analysis (Fig. 3 h), the effective removal of impurities, including Ti, Mn, Ni and Ca, made the obtained SNMS-800 more pure and more environmental friendly.

Based on the obtained results, the schematic diagram of different modification influence of MS-biochar was shown in Fig. 4. Summarily, single modification for MS-biochar with alkali or acid showed its boundedness for its adsorption property improvement. And the novel alkali-acid combination exhibited its superiority for MS-biochar' modification, including porosity enhancement and functional groups enrichment as well as impurities removal.

3.2. Effects of pyrolysis temperatures

As pyrolysis temperatures generally show a great influence for biochar properties, three calcination temperatures (400, 600 and 800 °C) of MS-biochar were taken into comparison. Intuitively, different from the completely black color of MS-600 and MS-800, MS-400 presented brownness, manifesting its imperfect carbonization. And with the pyrolysis temperature increasing from 400 to 800 °C, the productive rate of MS-biochar reduced from 72.4 to 58.3 wt%, which might be ascribed to the further loss of evaporable products acquired from thermal degradation reaction [23]. Simultaneously, higher temperature could facilitate the breakage of weak bonds along with more loss of hydrogen, nitrogen and oxygen [24], which might be an important reason for the BET increasing from 39.077 (MS-400) to 67.387 (MS-800) m^2/g (shown in Table 1), as well as the increasing pore volume. Despite the difference reflected in porosity, a lot of oxygen-containing functional groups ranging around 3000–3600 cm^{-1} on MS-400 disappeared with the calcination temperature increasing to 600 and 800 °C (shown in Fig. S1a). However, the TC adsorption capacity followed the order of MS-800 > MS-600 > MS-400, manifesting that the porosity of sludge biochar might play a more important role in TC adsorption. What's more, it has been proved that with the rising of calcination temperature, the obtained biochar owned relatively superior carbon content [25], and the aromatization degree of biochar increased [26], which might be the explanation of the reduced porosity of SNMS-400 and SAMS-400. And it can be speculated that the pore canals of lower aromatized biochar could easily collapse and be blocked during the alkali or acid modification process, which was validated with the pore size distribution (shown in Fig. 2a) and the shrinking BJH pore diameters. Clearly, the pyrolysis temperatures were closely related to adsorption properties of sludge biochar, which was similar with ramie biochar [27].

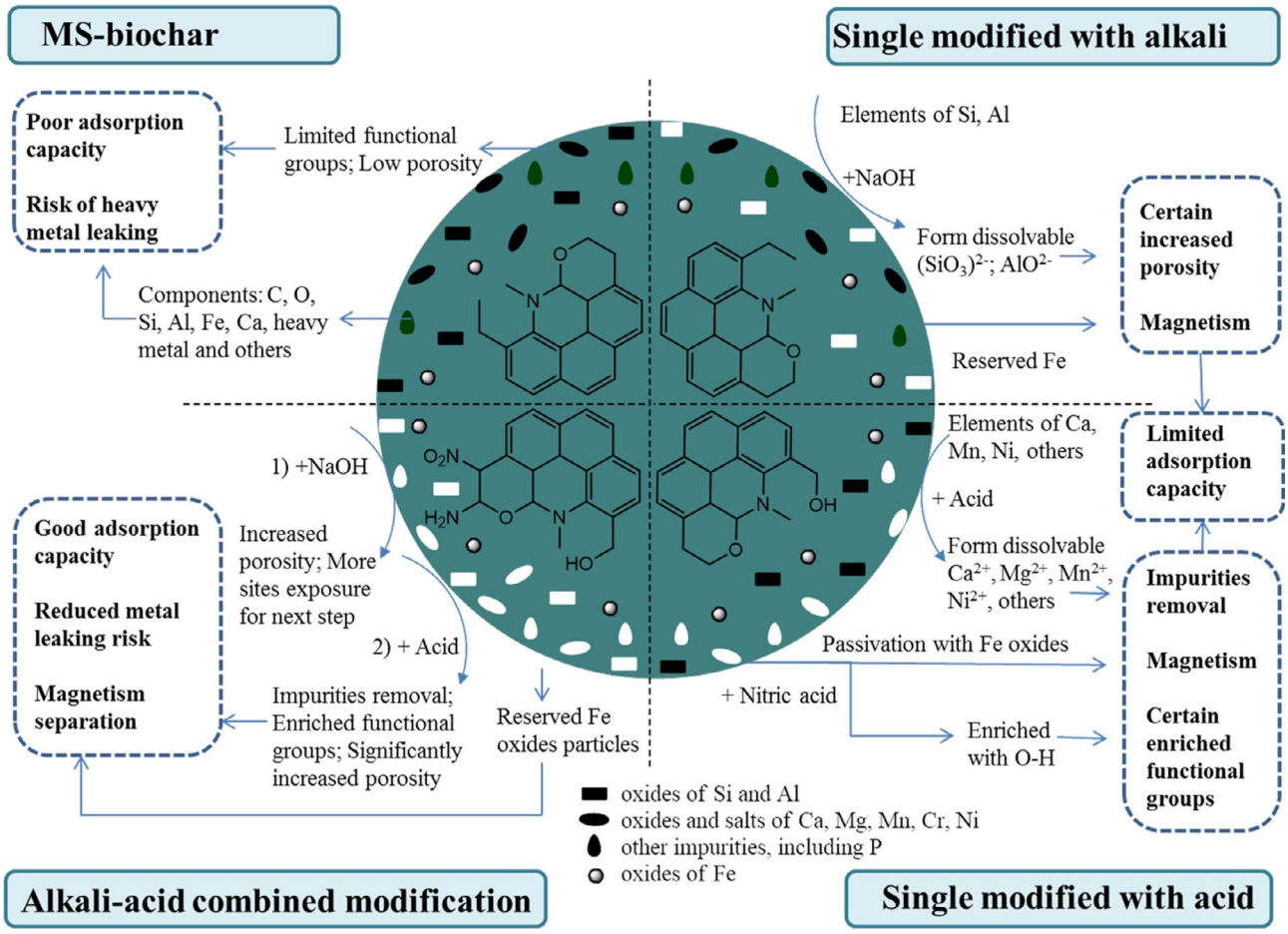

Fig. 4. The schematic diagram of different modification method for MS-biochar.

3.3. Effects of initial solution pH and ionic strength on TC adsorption

As pH value has prominent impacts on the existing forms, stabilities and characteristic absorption peaks of TC as well as the functional groups of adsorbent, it was regarded as a non-negligible factor for TC adsorption process [28]. Generally, for TC detection, despite of the existence of two characteristic absorption peaks (273 nm and 357 nm), the peak at 357 nm is regarded as a preferable and favorable choice. However, as shown in Fig. 5a, the characteristic absorption peaks could be affected by pH value. And under alkaline condition, the red shift phenomenon of adsorption peak from 357 nm to 380 nm was presented at pH 11. This is mainly because TC is relatively stable in acidic condition while easy to change under alkaline condition. Thereby, the UV–VIS spectrophotometry combined with TOC analysis was applied to ensure the accuracy of test results under alkaline solution.

The obtained results and corresponding zeta potential were shown in Fig. 5b. And the relative lowest removal efficiency (R) as 26.64% was observed at pH 3, along with a promptly increase to 52.63% at pH 4. Therewith, the optimal removal effect was reached at pH 7. With the gradually increasing pH from 8 to 12, the removal efficiency reduced slowly. The different dissociation constant (pKa = 3.3, 7.7 and 9.7) of TC determines its four kinds of existing forms in aqueous solution, cation (TC^+), molecule (TC^0), and anions (TC^- and TC^{2-}). In addition, the zero potential point (pH_{ZPC}) of SNMS-800 was around 3.47. The surface of SNMS-800 showed electropositive when pH < pH_{ZPC}. Therefore, there existed forceful repulsive interaction between the positively charged SNMS-800 and the cationic TC particles at pH 3. Along with the increased pH value from 4 to 7, the repulsive force sluggishly decreased, since TC mainly existed as molecular. Nevertheless, when pH value was > 7, the negatively charged SNMS-800 showed an incremental repulsion to anionic TC^- and TC^{2-}, along with a theoretical descending removal efficiency. Summarily, the electrostatic repulsion changed by pH could efficaciously affect TC adsorption on SNMS-800. And the good adsorption properties in a wide range of pH (from weak acid to neutral) demonstrated its advantage of broad applicability in real wastewater treatment [29].

Sodium chloride was added in TC adsorption system to investigate the effect of ionic strength. The concentration of sodium chloride varied from 0 to 0.1 M and the obtained results were presented in Fig. S2. Clearly, the adsorbed TC amount slightly reduced with the increasing sodium chloride concentration, manifesting that the electrostatic interaction was not the predominant interaction for TC adsorption by SNMS-800. Simultaneously, the trivial decrease might be attributed to the active sites competition on SNMS-800 between TC and sodium [30].

3.4. Adsorption kinetics

Adsorption is a time-dependent process. As for TC adsorption by SNMS-800 shown in Fig. S3a, the whole adsorption process could be divided into two parts: fast- and slow- adsorption stages, which were separated from the plot at 400 min. After the adsorption removal efficiency reached to 86% during fast adsorption stage, the adsorption rate rapidly reduced and gradually reached to equilibrium.

The obtained results analyzed by kinetics models were presented in Fig. S3 and Table S3. Compared to pseudo-first-order model, pseudo-second-order model showed a better fitting (R^2 = 0.998), demonstrating the adsorption rate was much affected by chemical mechanism [31]. Generally, adsorption behavior could be divided into two types, including surface adsorption and pore diffusion. Therefore, Evolich and Bangham models were applied for investigation. Accordingly, Evolich

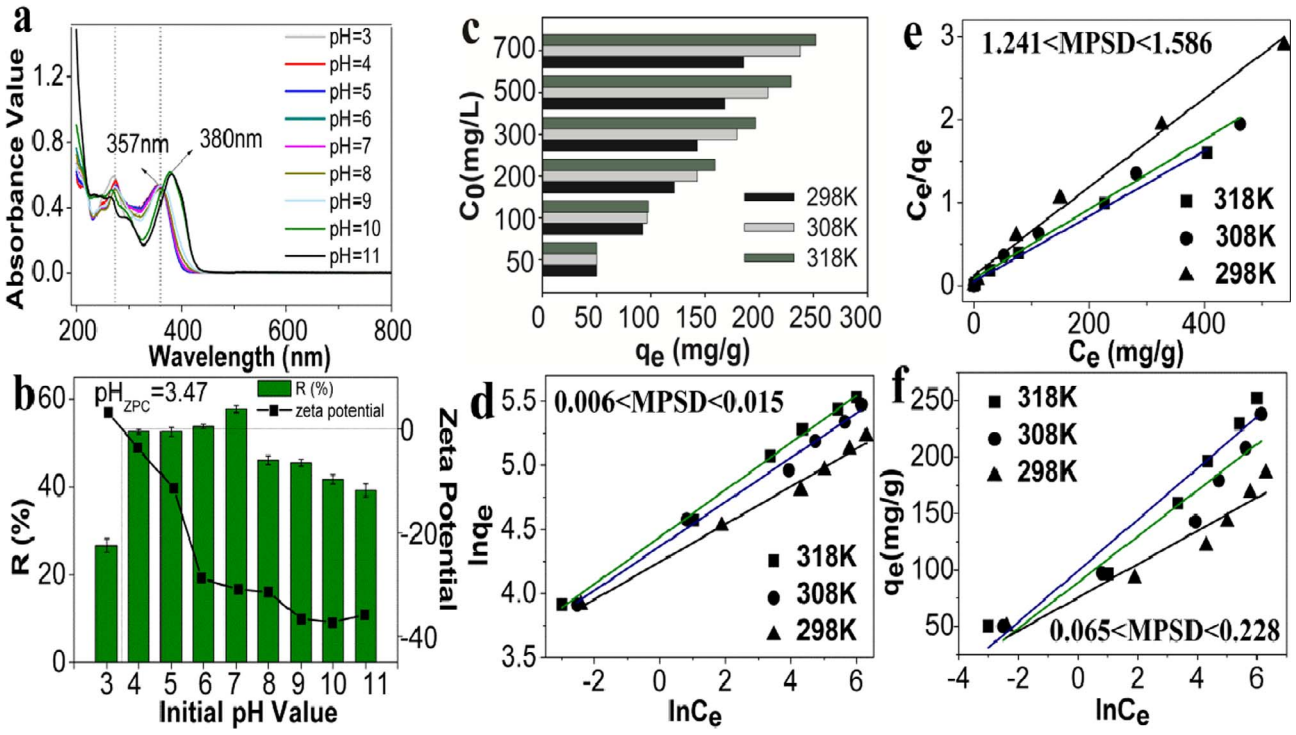

Fig. 5. UV–VIS full scan spectrum for TC at different pH values (**a**), effects of pH value on TC (C_0 = 200 mg/L) adsorption by SNMS-800 and zeta potential of SNMS-800 (**b**); Equilibrium adsorption capacity (**c**), Langmuir isotherm (**d**), Freundlich isotherm (**e**), and Temkin isotherm (**f**) of SNMS-800 on TC at different reaction temperature, where all goodness-of-fit indexes of isothermal models were measured by MPSD model.

model (R^2 = 0.99) reflecting comprehensive control of heterogeneous diffusion factors preferably fitted the dynamics data, where the rate constant (k_e = 20.462) reflected the adsorption speed. And relatively good linearity (R^2 = 0.967) of Bangham model revealed the existence of channel diffusion process for this adsorption process.

Moreover, intra-particle diffusion model, a typical empirical formula, was applied to explore the diffusion mechanisms, as well as the possible rate controlling procedure. And as shown in Fig. S3d and Table S4, the plots of q_t against $t^{1/2}$ were made up by three linear portions, none of which went through the coordinate origin indicating that diffusion within channel was not the only step in controlling the adsorption process [32]. The first fitting line section with a relatively steep slope (k_i = 4.777 mg/g·min$^{0.5}$) described the TC transportation to the SNMS-800 external surface from the solution which was controlled by the molecule diffusion and film diffusion. The second section corresponded to the slow adsorption stage (k_i = 1.312 mg/g·min$^{0.5}$), where the TC molecules diffused from the external surface to the internal pore structure of SNMS-800. The third section, along with a tardy slope (k_i = 0.533 mg/g·min$^{0.5}$), indicated the andante reaching of adsorption equilibrium. Conclusively, during the whole TC adsorption process, after originally being adsorbed to the surface of SNMS-800 controlled by molecule diffusion and film diffusion, the TC molecules then entered the internal pore structure of SNMS-800 under the effect of intra-particle diffusion, gradually adsorbed by the interior surface of SNMS-800 and finally reached to the adsorption equilibrium.

3.5. Adsorption isotherms

As presented in Fig. 5c, the equilibrium adsorption capacity of TC on SNMS-800 increased with the incremental reaction temperature and initial TC concentration. And four adsorption isothermal models, including Langmuir, Freundlich, Temkin and Dubinin-Redushckevich (D-R) models, were applied for adsorption mechanism investigation. All goodness-of-fit indexes of isothermal models were measured by MPSD model. All analyzed results were concluded in Table 2 and Fig. 5d–f.

As for Langmuir model, a good linear relationship ($0.986 \le R^2 \le 0.995$) was acquired with MPSD values ranging from 1.241 to 1.586, which assumed monolayer adsorption on a uniform surface with finite identical adsorption sites, demonstrating that chemical adsorption might play an important role for TC adsorption on SNMS-800. And the rising reaction temperature brought with the increased q_m and K_L values, manifesting that the higher temperature could promote the adsorption process by strengthening the bonding [33] between the TC and active sites of SNMS-800. The obtained values of separation factor (R_L) between 0 and 1 indicated its favorable [34].

Based on the Freundlich model which was suitable for multi-layer adsorption on non-uniform surface, a highly linear relationship ($0.989 \le R^2 \le 0.996$) with lower MPSD values ($0.006 \le$ MPSD ≤ 0.015) manifested its better description, demonstrating that TC adsorption by SNMS-800 might also closely associate with physical interaction. The values of the heterogeneity factor 1/n, representing the bond distribution, were all less than 1, indicating that the adsorption is facile and favorable [35]. In addition, the maximum adsorption capacity of SNMS-800 for TC was reaching to 286.91 mg/g at 318 K, which is much higher than many other adsorbents (shown in Table 3). Based on the both good linear fitting of these two typical models, it could be speculated that both chemical and physical interactions were significant for TC adsorption by SNMS-800.

For verification, Temkin model was used for the further analysis. And different from the Langmuir and Freundlich models, Temkin model assumes that adsorption energy decreases linearly with the surface coverage and is more applicable to chemical adsorption process. The actual experimental data complied with the Temkin model in a relatively small coverage range, where chemical adsorption took place. Therefore, the obtained comparatively weak linear relationships ($0.909 \le R^2 \le 0.934$; $0.065 \le$ MPSD ≤ 0.2281) manifested that the chemical adsorption was not the only dominated interaction for TC adsorption on SNMS-800. What's more, the D-R model (shown in Fig. S4), which does not assume a homogeneous surface, agrees more with the actual situation. The obtained mean free energy (E kJ/mol) values were less than 8, manifesting physical forces affect the adsorption

Table 2
The obtained results of isotherm models of TC adsorption on SNMS-800 at pH = 7.

Temperature (K)	Langmuir model		Freundlich model		Temkin model		D-R model	
298	R^2	0.988	R^2	0.989	R^2	0.909	R	0.784
	MPSD	1.317	MPSD	0.011	MPSD	0.086	MPSD	1.113
	q_m	187.266	q_m	185.104	K_T	14.754	q_m	154.965
	K_L	0.044	K_F	69.949	f	167.340	K_d	4.272
	R_L	0.236	1/n	0.147			E	0.342
308	R^2	0.986	R^2	0.989	R^2	0.922	R	0.837
	MPSD	1.586	MPSD	0.015	MPSD	0.065	MPSD	1.165
	q_m	238.095	q_m	248.110	K_T	20.383	q_m	192.235
	K_L	0.052	K_F	78.933	f	78.634	K_d	0.768
	R_L	0.376	1/n	0.173			E	0.807
318	R^2	0.995	R^2	0.996	R^2	0.934	R	0.921
	MPSD	1.241	MPSD	0.006	MPSD	0.228	MPSD	1.134
	q_m	253.807	q_m	286.913	K_T	22.680	q_m	210.304
	K_L	0.085	K_F	84.867	f	79.292	K_d	1.204
	R_L	0.291	1/n	0.184			E	0.645

mechanism.

Precisely, the results turned out that TC adsorption on SNMS-800 could be controlled by multiple mechanisms where both physisorption and chemisorption played important roles.

3.6. Thermodynamic analysis

Thermodynamic results analyzed by Gibbs-Helmholtz equation were presented in Table S5. The negative values of ΔG suggested that TC adsorption on SNMS-800 was spontaneous and endothermic. Moreover, with the temperature increasing, the ΔG (kJ/mol) values decreased from −1.173 to −4.423, manifesting the adsorption reaction was more feasible and favorable at a relatively higher temperature35. The positive ΔS value indicated that, during the whole adsorption process, the affinity and the randomness at the solid-liquid interphase increased. Furthermore, the Frumkin equation was applied for verification. The β value was attributed to the intensity of the interactions, and the value of ΔG was negative, consistent with the analysis results of thermodynamic analysis.

3.7. Removal mechanism

The UV–VIS spectroscopic spectra ranging from 200 to 800 cm^{-1} were shown in Fig. 7a. Obviously, during the whole reaction course, except for the two typical absorption peaks of TC, no other peaks emerged. And the synchronization decreasing of these two peaks without offset demonstrated that the TC removal was dominated by adsorption. What's more, further proof obtained from 3D EEMs was shown in Fig. S5. Analogously, no obvious fluorescence substance could be observed among the two spectrums. It manifested that possible degradation products, namely humic acids-like organic matter which had strong fluorescence effect [36], were not generated.

Consequently, the overall adsorption process could be postulated as a multilayer process, including the TC transportation and the external/surface/pore diffusion and final adsorption by SNMS-800. Additionally, the strong TC adsorption of SNMS-800 was attributed to two crucial interactions, including physisorption and chemisorption. The corresponding adsorption mechanism diagram along with its magnetic separation ability was shown in Fig. 6, and the magnetization curve was shown in Fig. S6. Correspondingly, the physical adsorption was dominated with pore filling effect attributing to the appropriate pore size distribution which endowed SNMS-800 as a tailor-made adsorbent for TC removal. And the significant enhanced porosity of SNMS-800 could provide more adsorption sites. The growing mesoporous could reduce the steric hindrance effect to promote the adsorption process. And as for the chemical adsorption interactions, based on the large graphite structure, the strong π-π stacking interaction [37] was considered as the dominant chemical driving force for the strong TC adsorption. And the existence of ketone and amino functional groups gave TC a strong ability to accept electronic. Meanwhile, the SNMS-800 owing the aromatic rings presented a forceful ability of electron donor to form the cation-π interaction with TC. Additionally, the hydrogen bonding force between TC and SNMS-800 could facilitate the adsorption process.

3.8. Application on real water samples and regenerability

The investigation of SNMS-800, MS-800 and RS-biochar adsorption properties on TC in deionized water, tap water and lake water were

Table 3
The maximal adsorption capacity of TC on different adsorbents.

Adsorbent	q_m (mg/g)	Isotherm model	Mechanism	Reference
Aerobic granular sludge	4.62	Langmuir	–	[38]
Sugarcane bagasse biochar	17.4	Pseudo-second-order	π–π electro-donor–acceptor (EDA) interaction	[39]
Bamboo charcoal	22.7	Langmuir	π-π EDA and cation-π interaction	[40]
Two microporous polymers	26.67/43.89	Langmuir	π–π stacking and π–π EDA interaction	[41]
Hydrothermal porous carbon	28.77	Freundlich	pore-filling effect and specific π–π interaction	[42]
Chitosan	53.82	Langmuir	functional groups in chitosan	[43]
Graphene oxide	73.53	Langmuir	π–π interaction and cation–π bonding	[44]
Granular activated carbon	85.29	Langmuir	Pore structure and high superficies reactivity	[45]
Rice husk biochar	86.21	Pseudo-second-order	functional groups	[46]
MeOH-biochar	101.01	Pseudo-second-order	π–π EDA interactions	[46]
Magnetic crosslinked resins	105.34	Langmuir	electrostatic attractions and π–π effects	[47]
Hydrogen titanate nanobelts	151.1	Langmuir	Surface complexation	[48]
Multi-walled carbon nanotubes	156.2	Freundlich	π–π interaction and cation–π bonding	[49]
SNMS-800	286.91	Freundlich	pore-filling effect, π-π stacking interaction	This work

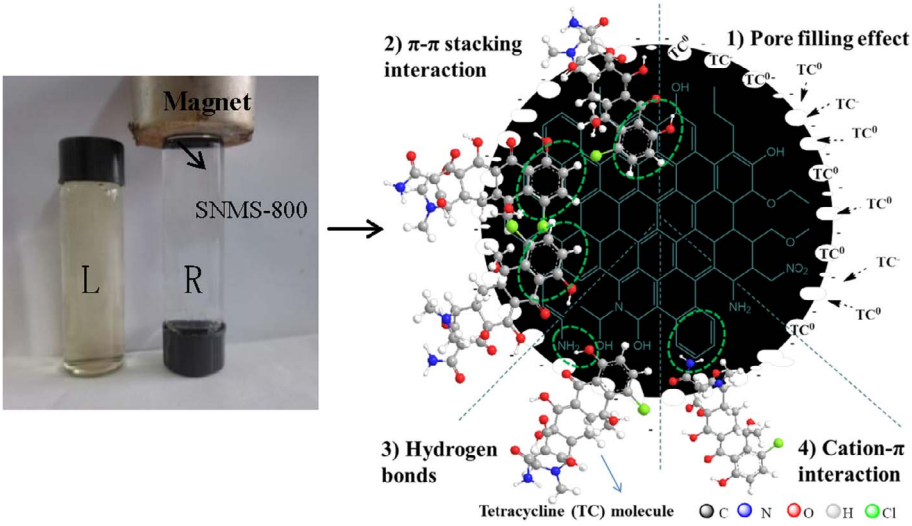

Fig. 6. TC adsorption mechanism diagram by SNMS-800 along with its magnetic separation ability (L: initial tetracycline solution; R: the same tetracycline solution treated with SNMS-800).

presented in Fig. 7b. Distinctly, among the three materials, SNMS-800 showed the best TC removal capacity along with the stable performance in tap and lake water.

Additionally, the hydraulic particle sizes of MS-800 and SNMS-800 were analyzed by Zeta-sizer Nano (ZEN3600, Malvern) with the Dynamic Light Scattering (DLS) method. The obtained data was shown in Table S6. Obviously, ascribing to the broken agglomeration of those magnetic biochars, their particle sizes sharply decreased after ultrasonic dispersion. And as for SNMS-800, its hydraulic particle size was larger than MS-800, which was attributed to its more plentiful porosity with stronger water-adsorption ability. The adsorbed water could expand its channel structure endowing SNMS-800 with a larger hydraulic particle size.

As shown in Fig. 7c, SNMS-800 indicated a good regeneration performance with slight decrease after five adsorption cycles, and after each cycle the adsorbents were magnetically separated. Compared with many other adsorbents shown in Table 3, SNMS-800 showed its high-adsorption capacity as well as its great low-cost advantages, which is of great importance for water treatment application on a large scale.

4. Conclusion

In conclusion, municipal sewage sludge biochar with effective alkali-acid combined modification was prepared with the significant increased BET area and porosity, along with oxygen-containing functional groups. The results demonstrated different modification methods and pyrolysis temperatures exerted remarkable influences on MS-biochars' properties, where MS-biochar modified with alkali-acid combined method and calcined at 800 °C (SNMS-800) showed optimum TC adsorption capacity. Additionally, the appropriate pore size distribution endowed SNMS-800 as a high-efficient adsorbent for the antibiotics removal. Multiple mechanisms involved among the adsorption process were dominated by π-π stacking interaction and strong pore filling effect, which manifested that appropriate multiple relation (1.7–6 times) between adsorbent's pore size and adsorbate size closely related to the adsorption strength and capacity, especially for large molecule organic matters. Besides the superior TC removal capacity, the extremely low cost, stable adsorption performance in natural water, good regeneration performance and magnetic separation ability entrust SNMS-800 with good potential for actual water restoration polluted with organic contaminations. Meanwhile, it provides a clue for materials modification starting with its specific components, and supplies a cost-effective way for

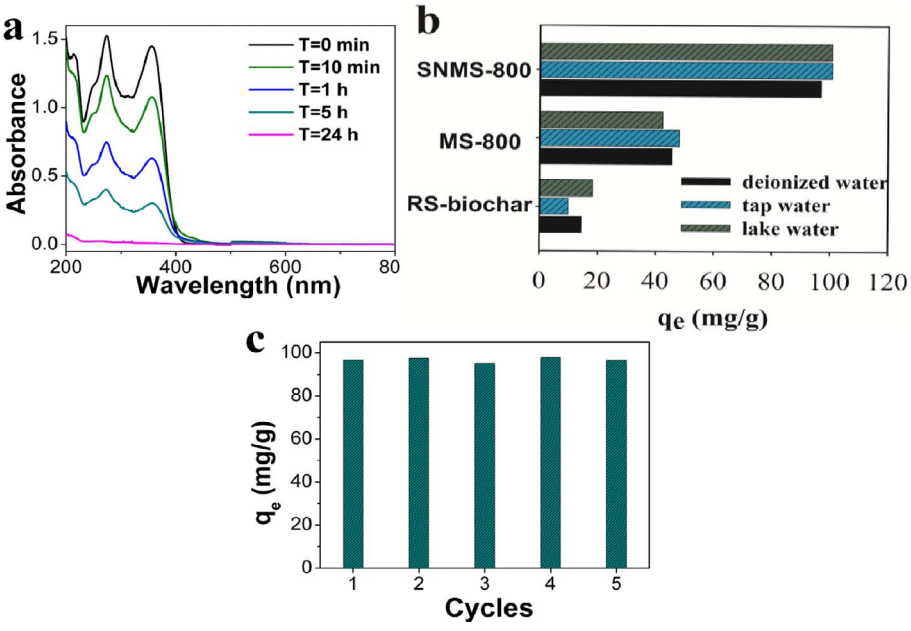

Fig. 7. The UV–VIS full scan spectrum of TC at different reaction time (**a**), TC (C_0 = 150 mg/L) adsorption by SNMS-800 in different water samples (**b**) and the corresponding regeneration test (**c**).

municipal sewage sludge resource disposal.

Notes

The authors declare no competing financial interest.

Acknowledgments

The study was financially supported by Projects 51579096, 51521006, 51222805, 51409024 and 51508175 supported by National Natural Science Foundation of China, the National Program for Support of Top-Notch Young Professionals of China (2012), the Program for New Century Excellent Talents in University from the Ministry of Education of China (NCET-11-0129).

Appendix A. Supplementary data

Supplementary data associated with this article can be found, in the online version, at http://dx.doi.org/10.1016/j.cej.2017.11.048.

References

[1] K. Kummerer, Antibiotics in the aquatic environment – a review – part II, Chemosphere 75 (2009) 435–441.
[2] K.A. Thompson, K.K. Shimabuku, J.P. Kearns, D.R.U. Knappe, R.S. Summers, S.M. Cook, Environmental comparison of biochar and activated carbon for tertiary wastewater treatment, Environ. Sci. Technol. 50 (2016).
[3] W.J. Liu, H. Jiang, H.Q. Yu, Development of biochar-based functional materials: toward a sustainable platform carbon material, Chem. Rev. 115 (2015) 12251.
[4] Y. Ying, B. Gao, W. Feng, C. Zhang, L. Yang, Engineered biochar from biofuel residue: characterization and its silver removal potential, ACS Appl. Mater. Interfaces 7 (2015) 10634.
[5] D. Cai, L. Wang, G. Zhang, Z. Xin, Z. Wu, Controlling pesticide loss by natural porous micro/nano composites: straw ash-based biochar and biosilica, ACS Appl. Mater. Interfaces 5 (2013) 9212.
[6] M. Lawrinenko, D.A. Laird, Anion Exchange Capacity of Biochar, Green Chem. 17 (2015) 4628–4636.
[7] S.J. Yuan, X.H. Dai, An efficient sewage sludge-derived bi-functional electrocatalyst for oxygen reduction and evolution reaction, Green Chem. 18 (2016).
[8] W.Q. Zuo, C. Chen, H.J. Cui, M.L. Fu, Enhanced removal of Cd(II) from aqueous solution using CaCO3 nanoparticle modified sewage sludge biochar, RSC Adv. 7 (2017) 16238–16243.
[9] J. Ifthikar, J. Wang, Q. Wang, T. Wang, H. Wang, A. Khan, A. Jawad, T. Sun, X. Jiao, Z. Chen, Highly efficient lead distribution by magnetic sewage sludge biochar: sorption mechanisms and bench applications, Bioresour. Technol. 238 (2017) 399.
[10] J.L. Hu, X.W. He, C.R. Wang, J.W. Li, C.H. Zhang, Cadmium adsorption characteristic of alkali modified sewage sludge, Bioresour. Technol. 121 (2012) 25–30.
[11] T. Lu, H. Yuan, Y. Wang, H. Huang, Y. Chen, Characteristic of heavy metals in biochar derived from sewage sludge, J. Mater. Cycles Waste Manage. 18 (2016) 725–733.
[12] K. Zhou, W. Zhou, X. Liu, Y. Wang, J. Wan, S. Chen, Nitrogen self-doped porous carbon from surplus sludge as metal-free electrocatalysts for oxygen reduction reactions, ACS Appl. Mater. Interfaces 6 (2014) 14911.
[13] L. Tang, Z. Xie, G. Zeng, H. Dong, C. Fan, Y. Zhou, J. Wang, Y. Deng, J. Wang, X. Wei, Removal of bisphenol A by iron nanoparticle-doped magnetic ordered mesoporous carbon, RSC Adv. 6 (2016) 25724–25732.
[14] P. Liu, W.J. Liu, H. Jiang, J.J. Chen, W.W. Li, H.Q. Yu, Modification of bio-char derived from fast pyrolysis of biomass and its application in removal of tetracycline from aqueous solution, Bioresour. Technol. 121 (2012) 235–240.
[15] W.J. Liu, F.X. Zeng, H. Jiang, X.S. Zhang, Preparation of high adsorption capacity bio-chars from waste biomass, Bioresour. Technol. 102 (2011) 8247–8252.
[16] J. Ling, T. Zhu, B. Xu, Study on preparation and coagulation properties of polyferric sulfate and polyacrylamide composite flocculants, 4th International Conference on Bioinformatics and Biomedical Engineering, Chengdu, China, 2010, pp. 1–4, , http://dx.doi.org/10.1109/ICBBE.2010.5517469.
[17] L. Tang, G.D. Yang, G.M. Zeng, Y. Cai, S.S. Li, Y.Y. Zhou, Y. Pang, Y.Y. Liu, Y. Zhang, B. Luna, Synergistic effect of iron doped ordered mesoporous carbon on adsorption-coupled reduction of hexavalent chromium and the relative mechanism study, Chem. Eng. J. 239 (2014) 114–122.
[18] G. Yang, L. Tang, Y. Cai, G. Zeng, P. Guo, G. Chen, Y. Zhou, J. Tang, J. Chen, W. Xiong, Effective removal of Cr(VI) through adsorption and reduction by magnetic mesoporous carbon incorporated with polyaniline, RSC Adv. 4 (2014) 58362–58371.
[19] H. Zhang, D. Fang, Z. Kong, J. Wei, X. Wu, S. Shen, W. Cui, Y. Zhu, Enhanced adsorption of phthalic acid esters (PAEs) from aqueous solution by alkylbenzene-functionalized polypropylene nonwoven and its adsorption mechanism insight, Chem. Eng. J. (2017).
[20] Y. Zhou, X. Liu, L. Tang, F. Zhang, G. Zeng, X. Peng, L. Luo, Y. Deng, Y. Pang, J. Zhang, Insight into highly efficient co-removal of p-nitrophenol and lead by nitrogen-functionalized magnetic ordered mesoporous carbon: performance and modelling, J. Hazard. Mater. 333 (2017) 80.
[21] W. Pei, H. Yin, Y. Liu, New development of carbon materials in environmental protection, Chongqing Environ. Sci. 25 (2003) 50–53.
[22] L. Ji, Y. Wan, S. Zheng, D. Zhu, Adsorption of tetracycline and sulfamethoxazole on crop residue-derived ashes: implication for the relative importance of black carbon to soil sorption, Environ. Sci. Technol. 45 (2011) 5580–5586.
[23] S. Thangalazhy-Gopakumar, S. Adhikari, H. Ravindran, R.B. Gupta, O. Fasina, M. Tu, S.D. Fernando, Physiochemical properties of bio-oil produced at various temperatures from pine wood using an auger reactor, Bioresour. Technol. 101 (2010) 8389–8395.
[24] M. Tripathi, J.N. Sahu, P. Ganesan, Effect of process parameters on production of biochar from biomass waste through pyrolysis: a review, Renewable Sustainable Energy Rev. 55 (2016) 467–481.
[25] M.I. Alwabel, A. Alomran, A.H. Elnaggar, M. Nadeem, A.R. Usman, Pyrolysis temperature induced changes in characteristics and chemical composition of biochar produced from conocarpus wastes, Bioresour. Technol. 131 (2013) 374–379.
[26] Y. Chen, H. Yang, X. Wang, S. Zhang, H. Chen, Biomass-based pyrolytic polygeneration system on cotton stalk pyrolysis: influence of temperature, Bioresour. Technol. 107 (2012) 411–418.
[27] L. Zhou, Y. Liu, S. Liu, Y. Yin, G. Zeng, X. Tan, X. Hu, X. Hu, L. Jiang, Y. Ding, Investigation of the adsorption-reduction mechanisms of hexavalent chromium by ramie biochars of different pyrolytic temperatures, Bioresour. Technol. 218 (2016) 351–359.
[28] L. Duan, L. Li, Z. Xu, W. Chen, Adsorption of tetracycline to nano-NiO: the effect of co-existing Cu(ii) ions and environmental implications, Environ. Sci. Processes Impacts 16 (2014) 1462.
[29] Z.H. Ruan, J.H. Wu, J.F. Huang, Z.T. Lin, Y.F. Li, Y.L. Liu, P.Y. Cao, Y.P. Fang, J. Xie, G.B. Jiang, Facile preparation of rosin-based biochar coated bentonite for supporting α-Fe O nanoparticles and its application for Cr(VI) adsorption, J. Mater. Chem. A 3 (2015) 4595–4603.
[30] W. Wei, S. Rong, C. Jing, Z. Wei, Removal of nitrobenzene from aqueous solution by adsorption on nanocrystalline hydroxyapatite, Desalination 263 (2010) 89–96.
[31] L. Tang, H. Feng, J. Tang, G. Zeng, Y. Deng, J. Wang, Y. Liu, Y. Zhou, Treatment of arsenic in acid wastewater and river sediment by Fe@Fe2O3 nanobunches: The effect of environmental conditions and reaction mechanism, Water Res. 117 (2017) 175.
[32] Z. Wu, H. Zhong, X. Yuan, H. Wang, L. Wang, X. Chen, G. Zeng, Y. Wu, Adsorptive removal of methylene blue by rhamnolipid-functionalized graphene oxide from wastewater, Water Res. 67 (2014) 330–344.
[33] L. Kong, L. Yan, Z. Qu, N. Yan, L. Li, β-Cyclodextrin stabilized magnetic Fe3S4 nanoparticles for efficient removal of Pb(II), J. Mater. Chem. A 3 (2015) 15755–15763.
[34] P. Wang, L. Tang, X. Wei, G. Zeng, Y. Zhou, Y. Deng, J. Wang, Z. Xie, W. Fang, Synthesis and application of iron and zinc doped biochar for removal of p -nitrophenol in wastewater and assessment of the influence of co-existed Pb(II), Appl. Surf. Sci. 392 (2017) 391–401.
[35] A. Bhatt, P. Sakaria, M. Vasudevan, R. Pawar, N. Sudheesh, H. Bajaj, H. Mody, Adsorption of an anionic dye from aqueous medium by organoclays: equilibrium modeling, kinetic and thermodynamic exploration, RSC Adv. 2 (2012) 8663–8671.
[36] W. Hou, X. Yuan, W. Yan, G. Zeng, H. Dong, X. Chen, L. Leng, Z. Wu, L. Peng, In situ synthesis of In_2S_3 @MIL-125(Ti) core–shell microparticle for the removal of tetracycline from wastewater by integrated adsorption and visible-light-driven photocatalysis, Appl. Catal. B Environ. 186 (2016) 19–29.
[37] L. Ji, W. Chen, L. Duan, D. Zhu, Mechanisms for strong adsorption of tetracycline to carbon nanotubes: a comparative study using activated carbon and graphite as adsorbents, Environ. Sci. Technol. 43 (2009) 2322–2327.
[38] K. Li, F. Ji, Y. Liu, Z. Tong, X. Zhan, Z. Hu, Adsorption removal of tetracycline from aqueous solution by anaerobic granular sludge: equilibrium and kinetic studies, Water Sci. Technol. A J. Int. Assoc. Water Pollut. Res. 67 (2013) 1490–1496.
[39] G. Li, W. Zhu, L. Zhu, X. Chai, Effect of pyrolytic temperature on the adsorptive removal of p-benzoquinone, tetracycline, and polyvinyl alcohol by the biochars from sugarcane bagasse, Korean J. Chem. Eng. 33 (2016) 2215–2221.
[40] P. Liao, Z. Zhan, J. Dai, X. Wu, W. Zhang, K. Wang, S. Yuan, Adsorption of tetracycline and chloramphenicol in aqueous solutions by bamboo charcoal: a batch and fixed-bed column study, Chem. Eng. J. 228 (2013) 496–505.
[41] F. Wang, F. Ren, P. Mu, Z. Zhu, H. Sun, C. Ma, C. Xiao, W. Liang, L. Chen, A. Li, Hierarchical porous spherical-shaped conjugated microporous polymers for the efficient removal of antibiotics from water, J. Mater. Chem. A (2017).
[42] X. Zhu, Y. Liu, C. Zhou, G. Luo, S. Zhang, J. Chen, A novel porous carbon derived from hydrothermal carbon for efficient adsorption of tetracycline, Carbon 77 (2014) 627–636.
[43] K. Jin, H. Liu, Y.M. Zheng, J. Qu, J.P. Chen, Systematic study of synergistic and antagonistic effects on adsorption of tetracycline and copper onto a chitosan, J. Colloid Interface Sci. 344 (2010) 117.
[44] E.E. Ghadim, F. Manouchehri, G. Soleimani, H. Hosseini, S. Kimiagar, S. Nafisi, Adsorption properties of tetracycline onto graphene oxide: equilibrium, kinetic and thermodynamic studies, PLoS One 8 (2013) e79254.
[45] P. Liu, Q. Wang, C. Zheng, C. He, Sorption of Sulfadiazine, Norfloxacin, Metronidazole, and Tetracycline by Granular Activated Carbon: Kinetics, Mechanisms, and Isotherms, Water Air Soil Pollut. 228 (2017) 129.
[46] X.R. Jing, Y.Y. Wang, W.J. Liu, Y.K. Wang, H. Jiang, Enhanced adsorption performance of tetracycline in aqueous solutions by methanol-modified biochar, Chem. Eng. J. 248 (2014) 168–174.
[47] M. Zhang, A. Li, Q. Zhou, C. Shuang, W. Zhou, M. Wang, Effect of pore size distribution on tetracycline adsorption using magnetic hypercrosslinked resins, Microporous Mesoporous Mater. 184 (2014) 105–111.
[48] W. Li, J. Wang, G. He, L. Yu, N. Noor, Y. Sun, X. Zhou, J. Hu, I.P. Parkin, Enhanced Adsorption Capacity of Ultralong Hydrogen Titanate Nanobelts for Antibiotics, J. Mater. Chem. A 5 (2016).
[49] Y. Fei, M. Jie, H. Sheng, Adsorption of tetracycline from aqueous solutions onto multi-walled carbon nanotubes with different oxygen contents, Sci. Rep. 4 (2014) 5326.